Engineering Journal issn: 0125-8281

Article

Virtual Oscillator Control of Multiple Solar PV Inverters for Microgrid Applications

Han Min Htut[a,*] **and Wijarn Wangdee**[b]

Electrical Power and Energy Engineering Program, The Sirindhorn International Thai-German Graduate School of Engineering, King Mongkut's University of Technology North Bangkok, Bangkok, Thailand

E-mail: [a]han.m-epe2017@tggs.kmutnb.ac.th (Corresponding author), [b]wijarn@ieee.org

Abstract. This paper proposes the inverter control strategy for multiple solar PV generation sources based on the two-stage converters with a combination of the modified virtual oscillator control (VOC) and the cascaded sliding mode control (SMC). With this proposed control strategy, the load power-sharing in proportion to the inverter rating is guaranteed when the solar PV output satisfies the power-sharing requirement. On the other hand, the control algorithm autonomously forces the solar PV to operate at the maximum power point if the solar PV output is lower than the power-sharing requirement. Various operating scenarios have been simulated to appreciate the effectiveness of the proposed control scheme for ensuring the load-power sharing and maintaining the voltage and frequency stability of the islanded microgrid containing a 100% solar PV generation.

Keywords: Cascaded sliding mode control (Cascaded SMC), distributed generation (DG), maximum power point tracking (MPPT), microgrid, photovoltaics (PV), virtual oscillator control (VOC).

ENGINEERING JOURNAL Volume 24 Issue 5
Received 30 December 2019
Accepted 3 July 2020
Published 30 September 2020
Online at https://engj.org/
DOI:10.4186/ej.2020.24.5.173

1. Introduction

Continuous increase in distributed generation (DG) sources in particularly from renewable energy sources embedded in distribution utility grids has progressively promoted the concept of microgrid applications to enhance environmental, economic and reliability goals from both customer's and utility's standpoints. Microgrid is a controllable small-scale power system that can be achieved by taking the advantage of integrating DG sources including energy storage systems (ESSs) and local load demand within a well-defined geographical boundary. Microgrids exist in both grid-connected and isolated forms with various sizes and configurations connected at low or medium voltage (LV/MV) levels. In both grid-connected and islanded operation modes, microgrids should maintain balance between generation and load demand, while satisfying certain reliability, power quality, and adequacy standards [1].

With significant penetration of solar photovoltaics (PV) generation due to dramatic cost reduction, ease of installation, less maintenance and long lifetime, the PV sources therefore become the most promising renewable energy sources [2]. However, variable solar power output with no inertia contribution from inverter-based generations has introduced various challenges for reliable grid operation under high penetration levels. Consequently, the electric power grid is on the edge of a paradigm shift due to the increasing penetration of inverter-based resources [3].

Due to the intermittent nature of the solar PV resources, the generated power output from these sources is always fluctuating while preferably operating them at the maximum power point (MPP) of the available PV sources to maximize the energy production [4]. In contrast, the maximum power point tracking (MPPT) operation will affect the stability of the microgrid under the high PV penetration [5] especially in the islanded mode operation where it is necessary to regulate the voltage and frequency of the microgrid to ensure its system integrity.

According to [6, 7], the energy storage systems (ESS) are introduced as the important part of the microgrid to ensure the energy balance (load/generation balance) by means of regulating voltage and frequency in an islanded microgrid consisting of variable solar PV generation. Although ESS could provide the simplest solution to address solar power fluctuation while meeting the load demand, this solution however comes with a considerable increase in system cost [8]. For this reason, different methods have been proposed in the literature to overcome these issues so as to avoid or minimize the utilization (or perhaps the size) of the ESS.

In [9], a hybrid controller with a switch between the so-called fast MPPT controller and the slow MPPT for microgrid-integrated PV sources was presented. The value of dP/dV is used as a threshold to control switching between the two controllers. The universal controller was proposed in [10] where there is a need of DC-link voltage regulation and MPPT control that are achieved autonomously without the requirement of the control system reconfiguration. The improved dual droop control scheme was proposed in [11] to control the two-stage converters with PV sources where the DC-link voltage of each converter is allowed to drop a little whenever the PV capacity cannot meet its droop command. By doing so, the droop power command is reduced in order to allow the converter with enough capacity to increase its generation to meet the load demand. In all the above literature, the decentralized control method known as the 'droop control' was utilized as the primary controller for the voltage source inverter (VSI).

Alternatively, the new decentralized control method known as the 'virtual oscillator control' (VOC) for the single-phase inverter and the three-phase inverter was introduced in [12, 13], respectively. This VOC method was used to ensure power-sharing and synchronization of parallel inverters in the islanded microgrids. The detailed design strategies for the virtual oscillator control is presented in [14]-[16] with the experimental validation using the hardware in the loop (real-time digital simulation). The VOC approach does not only provide the droop-like controls for voltage and frequency regulation in the steady-state operation, but this decentralized control method (VOC) also has some advantages over the droop control method such as less computational burden since it acts on instantaneous measurements, which leads to a faster and better damped response for dynamic performance [17]. Reference [18] introduced the solar PV sources interfaced through virtual oscillator controlled voltage source inverters with an addition of the MPPT control loop to VOC for microgrid applications. However, the energy storage system (ESS) is still required by this approach for maintaining the islanded microgrid voltage.

Inspiring from [10, 11], the two-stage converters are used to interface the solar PV sources, where the DC-link voltage regulation and MPPT are incorporated without the requirement for the control system reconfiguration. This paper enhances the above-mentioned method by utilizing the VOC approach to control the inverter instead of using the droop control as implemented in [10, 11]. Further inspired by [18] for using the VOC-based voltage source inverter (no DC-DC boost conversion stage) with the perturb & observe MPPT method, this paper alternatively proposes the VOC-based two-stage converters with the MPPT loop using the incremental conductance method to regulate the current scaling factor of the VOC in order to adjust power output of the inverter. Conclusively, the control strategy for multiple solar PV sources based on the two-stage converters, constituting DC-DC boost converters and VOC-based voltage source inverters, is proposed in this paper in order to achieve the MPPT whenever necessary while ensuring the load-power sharing and maintaining the voltage and frequency stability of the islanded microgrid containing a 100% solar PV generation regardless of the utilization of the energy storage system (ESS). The proposed control scheme is also applicable for the grid-connected mode of operation.

The salient operation features of this proposed control scheme are capable of successfully managing the two practical islanded operation conditions without the requirement of the control system reconfiguration, which are briefly described as follows:

1) When all PV generations are not constrained by solar irradiation, all the PV generations will automatically share their outputs to match the total island load. In this case, the operating points of all the PV generations may not be at MPP.
2) When one of PV generations is constrained by solar irradiation, it will operate at the MPP while the rest of PV generations (who are not constrained by the solar irradiation) will cover the remaining load.

The rest of this paper is organized as follow. Section 2 presents a test system for microgrid applications. In Section 3, the overall proposed control scheme is explained in details. Section 4 discusses the effectiveness of the proposed controller under five different operation scenarios considering both islanded and grid-connected modes where their simulation results are illustrated using the small-scale LV test system. Finally, the paper is concluded in Section 5.

2. Microgrid Test System

A configuration of the LV test system considered in this research is shown in Fig. 1. It consists of a microgrid with two parallel-connected DGs (i.e. named DG-1 and DG-2) to serve the microgrid load at the point of common coupling (PCC) while connecting to the main grid through a circuit breaker. The microgrid load is assumed to be a resistive load. Three-phase voltage source is considered as the main grid. The physical parameters of microgrid are given in Table 1. In Table 1, both DGs are solar PV power generations are different in size. The nominal voltage and frequency values are selected to represent a low voltage system. The use of the grid short-circuit value of 1.6 MVA is to represent the three-phase voltage source from the stiff grid. The pre-determined variations of voltage and frequency is selected as large values in order to observe the response of controller more clearly. However, with the proposed VOC, these values can also be chosen according to existing industry standards by recalculating the controller parameters based on [14]. The inverter output filter parameters are calculated according to [19].

In addition, a distribution line is modelled by a resistance (R_{line}) in series with an inductance (L_{line}) between each DG and PCC. V_{dc}, I_{dc}, i_L, $I_{f(abc)}$ are the DC-link voltage, current, inductor current of the boost converter, and the inductor current from LCL filter, respectively. The general schematic of the proposed inverter control strategy is also presented in Fig. 1. It composes of a cascaded SMC and modified VOC, which are explained in details in the next section. Note that DG-2 is double in size compared to DG-1, but it has the same control configuration and electrical connection as of DG-1.

Table 1. Test system parameters.

System Parameters		
Nominal voltage	400V	
Frequency	50Hz	
Switching frequency	15kHz	
Grid short-circuit power	1.6 MVA	
Microgrid Parameters		
Description	***DG-1***	***DG-2***
Rated power	15 kVA	30 kVA
Voltage variation(ΔV)	±10%	±10%
Frequency variation ($\Delta\omega$)	±10%	±10%
Inverter-side filter inductance	629 μH	314 μH
Load-side filter inductance	377 μH	189 μH
Filter capacitance	15 μF	30 μF
Line impedance(R_{line}, X_{line})	0.003 Ω, 0.003 Ω	0.003 Ω, 0.003 Ω
DC-link capacitance	4mF	8mF
DC-link reference voltage	800 V	800 V

DOI:10.4186/ej.2020.24.5.173

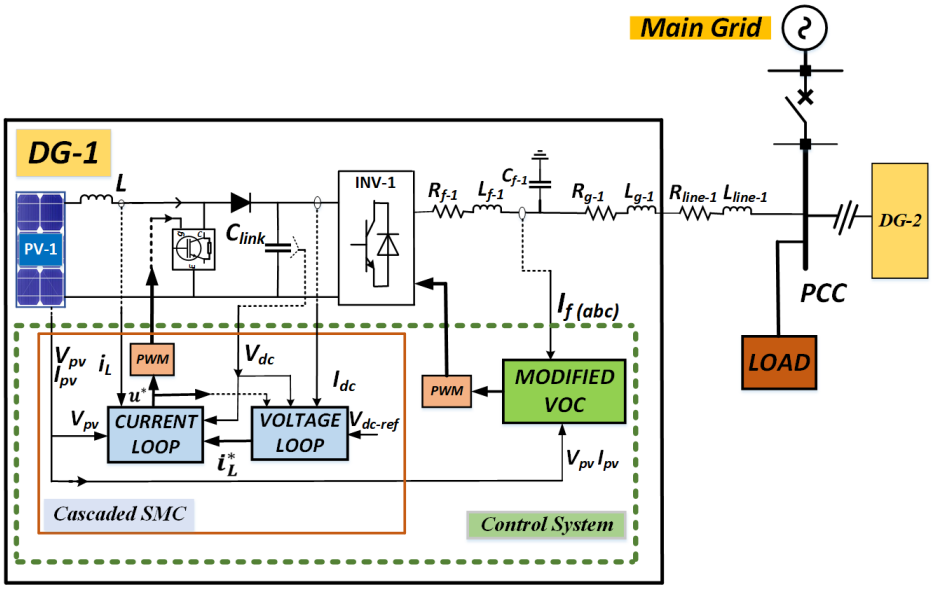

Fig. 1. Schematic diagram of the test system with the proposed control strategy.

3. Proposed Inverter Controller Design

In this section, the proposed inverter control scheme composing of the cascaded SMC and the modified VOC is presented. According to the control configuration from Fig. 1, the cascaded SMC is used to control DC-link voltage, whilst the modified VOC is designed to guarantee voltage and frequency regulation, and power-sharing under different load and solar irradiation conditions without the need of ESS. The control objectives of this paper are:

1) To guarantee the load power-sharing according to inverter rated power when the power output of the solar PV sources satisfy the power-sharing requirement.
2) To force the solar PV to operate in MPP mode if the power generation from solar PV is lower than the power-sharing requirement.

The detailed inverter controller design is explained in the following.

3.1. Cascaded Sliding Mode Control of DC-DC Boost Converter

The DC-DC boost converters are usually used in solar PV systems due to its simplicity and robustness. In boost converter with changing input voltage, the DC output voltage is needed to be controlled to achieve the desired value. The DC-DC boost converter with an ideal switch [20] is shown in Fig. 2.

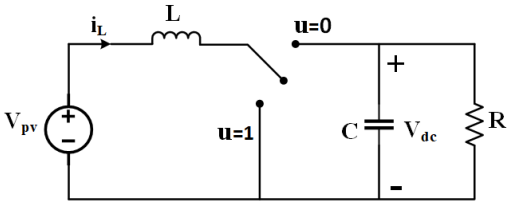

Fig. 2. DC-DC boost converter with an ideal switch.

In this paper, a cascaded sliding mode control (Cascaded SMC) is used to control the output voltage of the boost converter because of its superior dynamic, accuracy and robustness against internal and external disturbances [21, 22]. In general, the SMC is designed to force the system state variables onto the predefined sliding surface and then keep them close to a neighborhood of this surface.

By applying Kirchhoff's voltage and current laws, the dynamics of the boost converter is obtained as follows:

$$\frac{dV_{dc}}{dt} = \frac{-V_{dc}}{RC} + \frac{1}{C}(1-u)i_L \tag{1}$$

$$\frac{di_L}{dt} = \frac{V_{pv}}{L} - (1-u)\frac{V_{dc}}{L} \tag{2}$$

where R is the equivalent resistance at the output of the boost converter, u is the duty cycle signal used to control the converter.

The proposed Cascaded SMC scheme consists of two control loops (i.e. the inner current loop and the outer voltage loop) for regulating the DC output voltage of the boost converter. Robust sliding mode control based on reaching law method [23] is applied in this paper. For the inner current control loop, the sliding surface is chosen as:

$$S_I = K_{1-I}(i_L^* - i_L) + K_{2-I}\int(i_L^* - i_L)dt \tag{3}$$

where K_{1-I} and K_{2-I} are designed coefficients of the sliding surface, i_L^* is the current reference obtained from the output of the outer voltage control loop.

Taking time derivative of Eq. (3), then substituting $\frac{di_L}{dt}$ from Eq. (2) to Eq. (3), it yields:

$$\begin{aligned}\frac{dS_I}{dt} &= \frac{1}{L}\left(V_{dc}-V_{pv}\right)K_{1-I}+K_{2-I}\left(i_L^*-i_L\right)\\ &\quad -\frac{1}{L}K_{1-I}V_{dc}u = A_I - B_I u\end{aligned} \tag{4}$$

Let's define $A_I = \frac{1}{L}\left(V_{dc}-V_{pv}\right)K_{1-I}+K_{2-I}\left(i_L^*-i_L\right)$ and $B_I = \frac{1}{L}K_{1-I}V_{dc}$ for the sake of simplicity. Also, the reaching law with constant rate is chosen as shown in (5).

$$\frac{dS_I}{dt} = -K_{3-I}sat\left(S_I\right) \tag{5}$$

where: $$sat\left(S_I\right) = \begin{cases} sign\left(S_I\right) & if\ S_I > \phi \\ S_I/\phi & if\ S_I \le \phi \end{cases} \tag{6}$$

In this case, $sign\left(S_I\right)$ is a signum function of S_I. The value of ϕ parameter is selected with respect to the thickness of the chattering. In this paper, ϕ is chosen as 0.5 to maintain the trade-off between system performance and robustness of the proposed controller against uncertainties.

From Eq. (4) and Eq. (5), the control law for the inner current loop can be derived as in Eq. (7).

$$u = \frac{1}{B_I}\left\{A_I + K_{3-I}sat\left(S_I\right)\right\} \tag{7}$$

In the following, the Lyapunov stability criterion to analyze the stability of the proposed inner current control loop is applied. The Lyapunov function can be chosen as follows:

$$V = \frac{1}{2}S_I^2 \tag{8}$$

Taking the derivative of V with respect to time, it yields:

$$\begin{aligned}\frac{dV}{dt} &= S_I\frac{dS_I}{dt} = -S_I K_{3-I}sat\left(S_I\right)\\ &= -K_{3-I}\left|S_I\right|\end{aligned} \tag{9}$$

From Eq. (8) and Eq. (9), it can be seen that with $K_{3-I} > 0$, the Lyapunov function and its time derivative is positive definite and negative semi-definite, respectively. Hence, the proposed inner current loop is asymptotically stable.

Similarly, the sliding surface for the outer voltage loop is defined as:

$$S_V = K_{1-V}\left(V_{dc}^* - V_{dc}\right) + K_{2-V}\int\left(V_{dc}^* - V_{dc}\right)dt \tag{10}$$

Taking time derivative of Eq. (10), then substituting $\frac{dV_{dc}}{dt}$ from Eq. (1), it yields:

$$\begin{aligned}\frac{dS_V}{dt} &= \frac{V_{dc}K_{1-V}}{RC} + K_{2-V}\left(V_{dc}^* - V_{dc}\right) + \frac{(u-1)}{C}i_L\\ &= A_V - B_V i_L\end{aligned} \tag{11}$$

Let's define $A_V = \frac{V_{dc}K_{1-V}}{RC} + K_{2-V}\left(V_{dc}^* - V_{dc}\right)$ and $B_V = -\frac{(u-1)}{C}$ for the sake of simplicity. In order to reduce the chattering characteristics of the SMC, the combination of reaching law with constant rate and with power rate [23] is applied as:

$$\frac{dS_V}{dt} = -K_{3-V}sat\left(S_V\right) - K_{4-V}\left|S_V\right|^{K_{5-V}}\ sat\left(S_V\right) \tag{12}$$

where: $$sat\left(S_V\right) = \begin{cases} sign\left(S_V\right) & if\ S_V > \phi \\ S_V/\phi & if\ S_V \le \phi \end{cases} \tag{13}$$

From Eq. (11) and Eq. (12), the control law for the outer voltage loop is derived as in Eq. (14):

$$i_L = \frac{1}{B_V}\left\{A_V + K_{3-V}sat\left(S_V\right) + K_{4-V}\left|S_V\right|^{K_{5-V}}\ sat\left(S_V\right)\right\} \tag{14}$$

Applying the Lyapunov stability criterion, the stability of the proposed voltage control loop is analyzed by choosing the Lyapunov function as:

$$W = \frac{1}{2}S_V^2 \tag{15}$$

Taking the derivative of W with respect to time, it yields:

$$\begin{aligned}\frac{dW}{dt} &= S_V\frac{dS_V}{dt}\\ &= -K_{3-V}S_V sat\left(S_V\right) - K_{4-V}\left|S_V\right|^{K_{5-V}}\ S_V sat\left(S_V\right)\end{aligned} \tag{16}$$

From Eq. (15) and Eq. (16), it can be seen that the Lyapunov function is positive definite and its time derivative is negative semi-definite with $K_{3-V} \ge 0$ and $K_{4-V} \ge 0$. Therefore, the proposed voltage control loop is asymptotically stable.

3.2. Modified Virtual Oscillator Controller

The modified VOC utilized in this paper is shown in Fig. 3. This control logic measures the inverter output filter inductor current $i_{f\alpha}$ whereas its output v^*_{voc} is used to generate the PWM modulation signals. The oscillator consists of a negative damping resistor R_{voc}, a resonant $L_{voc}C_{voc}$ circuit that sets the system frequency and a nonlinear cubic voltage-dependent current source for sustaining the oscillation.

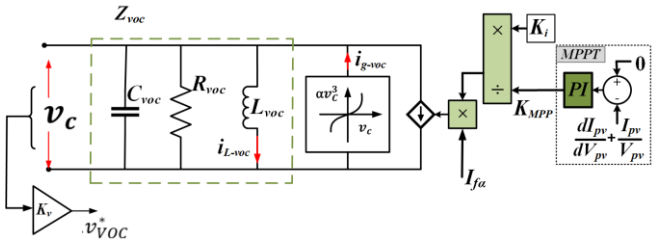

Fig. 3. Schematic diagram of modified VOC.

Applying Kirchhoff's voltage and current laws, the dynamics of the VOC are obtained as follows:

$$L_{voc}\frac{di_{L-voc}}{dt}=\frac{v_c}{K_v} \tag{17}$$

$$C_{voc}\frac{dv_c}{dt}=-\alpha\frac{v_c^3}{K_v^2}-\sigma v_c-K_v i_{L-voc}-K_v K_i i_{f\alpha} \tag{18}$$

where

- K_v, K_i are voltage and current scaling factors.
- $\sigma=\dfrac{1}{R_{voc}}$

Differentiating Eq. (18) and substituting Eq. (17), the VOC dynamics can be rearranged as:

$$\frac{d^2}{dt^2}v_c=\varepsilon\omega\sigma\left(1-\beta v_c^2\right)\frac{d}{dt}v_c-\omega^2 v_c-\varepsilon\omega K_i\frac{d}{dt}i_{f\alpha} \tag{19}$$

where $\beta:=\dfrac{3\alpha}{\sigma}$, $\varepsilon:=\sqrt{\dfrac{L_{voc}}{C_{voc}}}$, $\omega:=\dfrac{1}{\sqrt{L_{voc}C_{voc}}}$

The determination of parameters for VOC is adopted from [14] and the necessary equations and procedure are presented briefly in the following.

1) First, the maximum and minimum voltage limits are defined as V_{max} and V_{min}. The scaling factors are chosen based on $K_v=V_{max}$ and $K_i=3V_{min}/P_{rated}$.
2) The conductance $\sigma=\dfrac{V_{max}}{V_{min}}\dfrac{V_{max}^{\ 2}}{V_{max}^{\ 2}-V_{min}^{\ 2}}$ and the coefficient of cubic current source $\alpha=2\sigma/3>0$ are selected.
3) It is needed to satisfy the angular frequency $\omega_n=\left(\sqrt{L_{voc}C_{voc}}\right)^{-1}$ and the resistance $R_{voc}\geq\sigma^{-1}$ when choosing R_{voc}, L_{voc} and C_{voc} values in addition to maximum frequency variation $\Delta\omega$, the maximum rise time (t_{max}^{rise}) and the maximum ratio of third to first harmonics (δ_{max}).
4) If the voltage and frequency become out of predetermined limits with the change in load, the above steps needed to repeat (i.e. re-tune).

As we can see from Fig. 3, in order to utilize universal control purposes, the MPPT control algorithm based on incremental conductance (IC) method is used to modify the current scaling factor K_i. The basic of IC-MPPT algorithm is presented in Fig. 4, in which the solar PV sources will operate at the MPP if the ratio dP_{pv}/dV_{pv} satisfies [24, 25] with the condition expressed in Eq. (20).

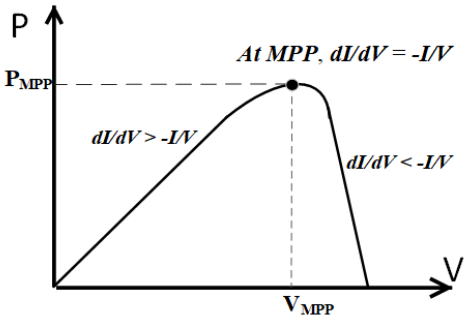

Fig. 4. Basic of IC-MPPT on P-V curve.

$$\frac{dP_{pv}}{dV_{pv}}=0 \tag{20}$$

Manipulating Eq. (20), it yields:

$$\frac{dP_{pv}}{dV_{pv}}=\frac{d\left(V_{pv}I_{pv}\right)}{dV_{pv}}=I\frac{dV_{pv}}{dV_{pv}}+V\frac{dI_{pv}}{dV_{pv}}=I+V\frac{dI_{pv}}{dV_{pv}} \tag{21}$$

At MPP, one can rewrite Eq. (20) as:

$$\frac{dI_{pv}}{dV_{pv}}+\frac{I_{pv}}{V_{pv}}=0 \tag{22}$$

A PI controller is implemented to satisfy Eq. (22), then its output K_{MPP} is used to modify the current scaling factor K_i in order to adjust inverter power output based on different solar irradiation. Inspiring from the natural characteristics of VOC, where the inverter power output is inversely proportional to the current scaling factor, the modified input of the VOC will be $I_{f\alpha}^{'}=\left(K_i/K_{MPP}\right)I_{f\alpha}$.

4. Simulation Results and Discussions

The effectiveness of the proposed inverter control strategy is validated in MATLAB/Simulink under different operating conditions and the simulation results are shown in this section.

The control parameters (after tuning) are summarized as follow, in which the gains of the Cascaded SMC and PI controller have been tuned based on a trial and error method:

- VOC Controller: Oscillator Parameters: R_{voc} =270mΩ, L_{voc} =52.08μH, C_{voc} =194.5mF, Voltage and current scaling factors: K_v =254.03, K_i =0.042.
- CSMC Controller: K_{1-I} =0.083, K_{2-I} =1.43, K_{3-I} =130, K_{1-V} =0.56, K_{2-V} =7.6, K_{3-V} =0.188, K_{4-V} =1, and K_{5-V} =0.5.
- PI Controller: K_p =10, K_I =150.

The IEC/ISO 62264 international standard [26] is applied to assess the microgrid operation with the proposed controller. The proposed VOC control method presented in this paper belongs to the zero level and first level of the IEC/ISO 62264. In order to satisfy the standard, five different operating scenarios (case studies) are simulated covering the microgrid operation in both islanded mode and grid-connected mode. The studies aim at examining whether or not the proposed system meets the standard under different circumstances such as change of solar radiation, load variation and so on. Meanwhile, it is also necessary to make sure that the power output sharing between each inverter when operating in different scenarios must be in accordance with the available output power. These five study cases illustrated in this section are described as follows:

1) **Case-A**: Power-sharing between two DGs with high solar irradiation
2) **Case-B**: Power-sharing between two DGs when one DG having high solar irradiation while another DG having low solar irradiation
3) **Case-C**: Islanded microgrid dynamics under load variations
4) **Case-D**: Microgrid performance during a seamless transition from grid-connected mode to intentional islanded mode
5) **Case-E**: Microgrid response to solar irradiation changes under grid-connected mode

4.1. Case-A: Power-Sharing between Two DGs with High Solar Irradiation

This scenario is based on the islanding operation of the microgrid where both DGs have sufficient power output (i.e. high solar irradiation) to supply the island load. The load is assumed constant at 30 kW throughout a 10-second period. The variation (reduction) of the solar irradiation is occurred at t = 3 second and t = 7 second on the DG-2 and on the DG-1, respectively. As shown in Fig. 5, both solar PV sources are receiving the abundant solar irradiation of 1000 W/m² initially (at t = 1s), which are more than enough to serve the total island load (30 kW) and therefore both DGs provide power-sharing according to their rated capacities (i.e. 10 kW output by DG-1 and 20 kW output by DG-2).

At t = 3s, the solar irradiation of DG-2 is reduced to 700 W/m². However, since the power output of DG-2 at that instant (P_{MPP-2} ≈ 21 kW at 700 W/m²) is still higher than the power-sharing requirement, thus the power-sharing ratio of two DGs remains unchanged. Similarly, at t = 7s when the solar irradiation of DG-1 is reduced to 800 W/m², the power output of DG-1 at this instant (P_{MPP-1} ≈ 13.8 kW at 800 W/m²) is still higher than the power-sharing requirement. As a result, the power-sharing ratio of two DGs remains unchanged even with the solar irradiation change on both DGs. Throughout the simulation, the DC-link voltages are maintained at 800 V by the designed Cascaded SMC and the inverter output voltages are also within the predefined limits. This confirms that the two DGs can share the load with respect to their rated capacities as long as the generated power of the two solar PVs satisfy the power-sharing requirement. It is worth emphasizing that in this operating scenario (Case-A) both DGs are not constrained by the available solar irradiation, and therefore they are not necessary to operate at their maximum possible generated power outputs. In other words, with the proposed inverter control scheme, both DGs are operating at the power output, which is lower than their MPP, based on the power-sharing ratio for just meeting the load in this case.

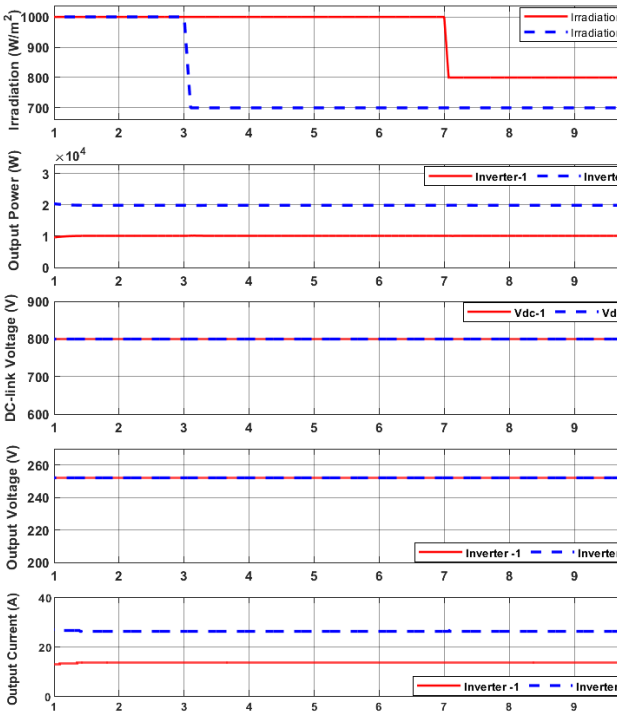

Fig. 5. Simulation results for Case-A.

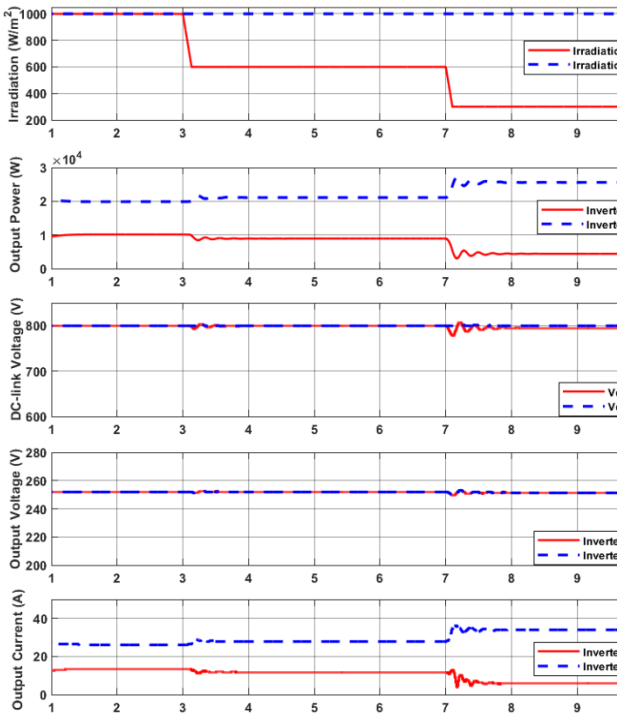

Fig. 6. Simulation results for Case-B.

4.2. Case-B: Power-Sharing between Two DGs When One DG Having High Solar Irradiation While Another DG Having Low Solar Irradiation

This scenario is based on the islanding operation of the microgrid when one of the DGs does not have sufficient power output (i.e. due to low solar irradiation) to fulfill the power-sharing requirement. The load is assumed constant at 30 kW throughout a 10-second period. The objective of this case study is to verify the performance of the proposed control scheme that forces the DG to operate in MPPT mode when its generated power output cannot meet the power-sharing requirement.

As illustrated in Fig. 6, both solar PV sources are initially receiving the abundant solar irradiation of 1000 W/m² initially. Later, the solar irradiation variation of DG-1 is occurred at t = 3s (decreasing to 600 W/m²) and then at t = 7s (decreasing to 300 W/m²), whereas the solar irradiation for DG-2 is abundant and remains constant throughout a 10-second period. At t = 3s where the solar irradiation of DG-1 reduced to 600 W/m², the DG-1 is forced to operate at its corresponding MPP of 8.9 kW (P_{MPP-1} at 600 W/m²) when it is not possible to meet its power-sharing requirement. As a result, DG-2 is automatically generating more power output (1.1 kW increase) to cover the power drop from DG-1. Likewise, at t = 7s, the DG-1 is further forced to operate at its corresponding MPP of 4.4 kW (P_{MPP-1} at 300 W/m²) and therefore DG-2 power output is automatically increased to operate at 25.6 kW in order to meet the island load. The DC-link voltage suffers a short transient during solar irradiation changes. The longer transient period happens when the solar irradiation of DG-1 is reduced to 300 W/m², which requires the larger increase in power generation requirement from DG-2. The output voltages of both inverters are kept within the predefined limits. The results show that the proposed control strategy can autonomously switch between two operating modes (i.e. from power-sharing to the MPP when reaching the constraint) without the need of the inverter control scheme reconfiguration.

4.3. Case-C: Islanded Microgird Dynamics under Load Variations

In this study scenario, the solar irradiations for both DGs remain constant throughout a 10-second period. In contrast, the island load is initially set at 25 kW and then is varied to 40 kW at t = 3s (i.e. representing a load addition), later dropped down to 3 kW at t = 6s (i.e. representing a large load tripping), and afterwards returned back to 25 kW at t = 9s (i.e. representing a load restoration).

As it can be observed from Fig. 7, with the island load variations, the two DGs effectively provide the power-sharing in proportion to their respective rated power in order to meet the island load at any instant. The DC-link voltage shows a transient with the sudden drop of load to 3 kW, and then returns back to steady-state shortly. Nevertheless, the RMS voltage outputs of each DG are still kept with the predefined limit in the entire simulation period. Therefore, it can be concluded that the proposed control method can remarkably perform the voltage regulation function to maintain the microgrid voltage, which is considered to be one of the most advantages for utilizing VOC concept in this case.

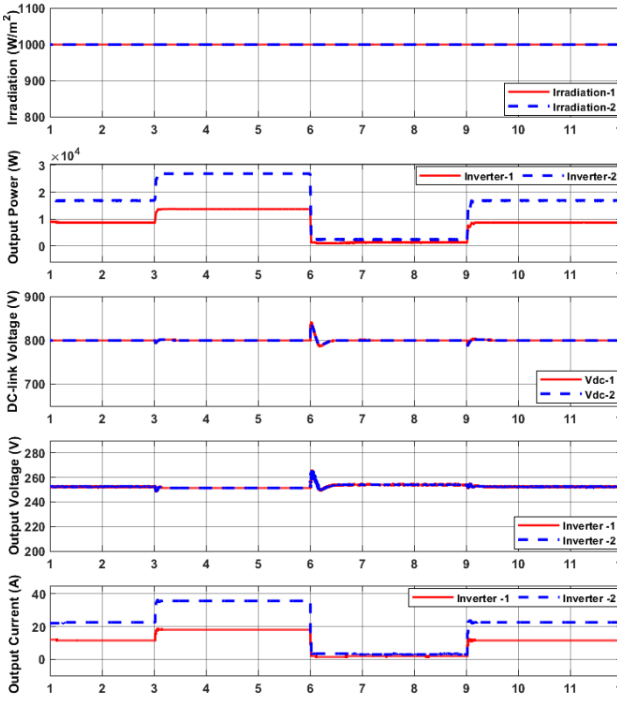

Fig. 7. Simulation results for Case-C.

4.4. Case-D: Microgrid Performance During a Seamless Transition from Grid-Connected Mode to Intentional Islanded Mode

This scenario investigates the microgrid dynamic performance during a transition from the grid-connected mode to the islanded mode. In this case, the microgrid load remains constant at 18 kW throughout a 10-second period. Also, the solar irradiation of the two DGs are kept constant at 1000 W/m² and therefore the combined power generation is 45 kW (i.e. 15 kW from DG-1 and 30 kW from DG-2). Initially, the microgrid is connected to the main grid where the two DGs serve as the grid-feeding inverters to inject the excess power to the main grid.

As illustrated in Fig. 8, at t = 4s, the circuit breaker at the PCC is opened for an intentional islanded operation. Immediately right after the opening of the circuit breaker, the two DGs returns to the power-sharing mode to solely take care of the island load according to their rated capacities. During the grid-connected mode, the voltage at the PCC (also at the inverters' terminal) is at the same level as the grid voltage. However, when transitioning to the islanded mode, the voltage at the PCC is regulated within the predefined limits by the VOC inverters from both DGs. The frequency of the island also remains constant throughout the simulation except with a small transient during the instant of intentional islanding. This frequency regulation is another key advantage of utilizing the VOC approach. It should be noted that the transient values occurred during the transition from the grid-connected to the islanded mode in Case-D as presented in Fig. 8 are also complied with the IEEE 1547 standard [27, 28].

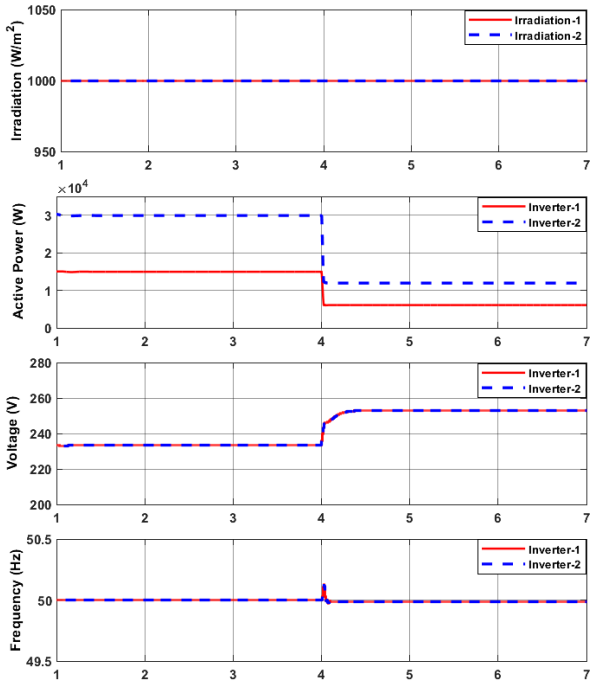

Fig. 8. Simulation results for Case-D.

4.5. Case-E: Microgrid Response to Solar Irradiation Changes under Grid-Connected Mode

In this scenario, a 24 kW constant load is connected at the PCC while the microgrid is operating in grid-connected mode. In this mode of operation, the excess power generation from both DGs (i.e. under high solar irradiation conditions) will be fed into the main grid. Conversely, the main grid will supply and additional power to the microgrid if there exists in the power shortage generated by both DGs (i.e. under low solar irradiation conditions).

As shown in Fig. 9, both DGs are initially generating the power at their maximum capacities (i.e. 15 kW from DG-1 and 30 kW from DG-2) under the high solar irradiation at 1000 W/m². At t = 3s, the solar irradiation of DG-1 is reduced to 600 W/m² causing its power output dropped to 8.9 kW (P_{MPP-1} at 600 W/m²). Afterwards, at t = 7s, the power output of DG-2 is also decreased to 24 kW due to the solar irradiation reduction (P_{MPP-2} at 800 W/m²). According to the simulation results, the voltage measured at the PCC remains the same as the grid voltage with the fast transient response during solar irradiation changes. The frequency measured at the inverters is also held constant at 50 Hz with relatively very little transient during the solar irradiation changes due to the fact that the main grid can effectively maintain the grid frequency.

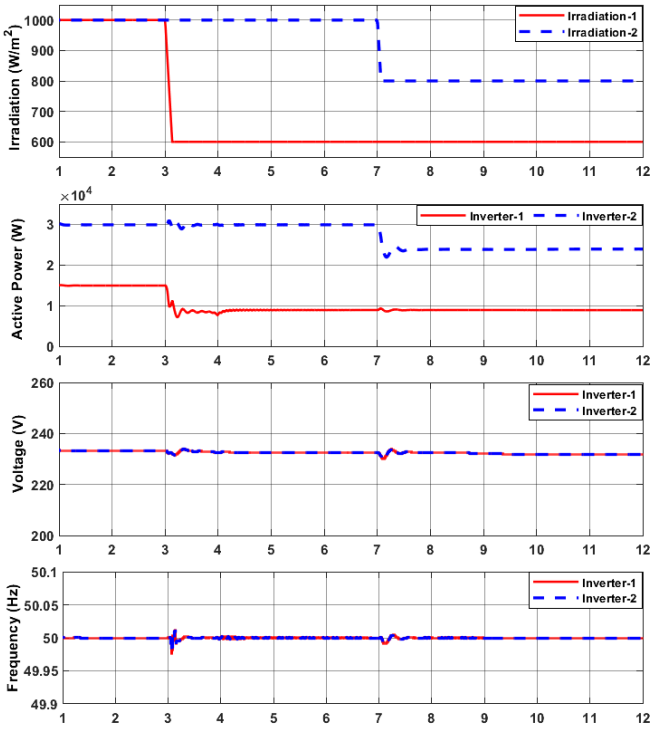

Fig. 9. Simulation results for Case-E.

It is worth emphasizing that the proposed inverter control strategy for operating multiple solar PV generations in the islanded mode (as presented in Case-A to Case-D) can perform effectively and adequately as long as the prime energy sources (solar irradiation) are available without utilizing the energy storage system (ESS). The

reliability in such a microgrid would improve to some extent in particularly when the grid disturbances occurred (causing the islanding operation) during the high solar irradiation, the microgrid can survive without the need of ESS in such a case. However, when there is low solar irradiation situations or in the night time and the disturbance occurred, such a microgrid unquestionably requires the ESS (if being islanded) in order to balance the load so that the microgrid voltage and frequency can be maintained. Nonetheless, the VOC-based inverter control strategy proposed in this paper is definitely also applicable for implementing on the ESS (i.e. battery) as the prime energy source besides the solar PV sources.

In addition, it should be noted that this paper presents a theoretical proof for the proposed concept with the simulation results. An extension of the proposed concept on the hardware-in-the-loop experiment would be augmented as the future research work in order to demonstrate an effectiveness of the proposed concept in practice.

5. Conclusion

This paper proposes a new control scheme for controlling solar PV generations for microgrid operation. A cascaded sliding mode control is applied to regulate the DC-link output voltage of the boost converters, while an incremental conductance based MPPT method to track maximum power is combined with the VOC-based inverter to allow the solar PV generations to operate at different control modes without the requirement for the control system reconfiguration.

The simulation results indicate that the proposed inverter control strategy can satisfactorily provide the load power-sharing among the inverters in proportion to the inverter rated power capacities as long as the available solar PV power generation satisfies the power-sharing requirement. Moreover, the modified VOC-based inverter effectively forces the solar PV generation to operate at the MPP when the available power output deems below the power-sharing requirement due to the solar irradiation drop. Regarding to power quality, the inverter voltage can be well maintained within the predefined limit during the islanding operation as well as being capable of following the grid voltage during the grid-connected operation.

References

[1] M. Farrokhabadi, "Microgrid stability, definitions, analysis, and modeling," IEEE Power and Energy Society, Technical Report PES-TR66, April 2018.

[2] F. A. Farret and M. G. Simoes, *Integration of Alternative Sources of Energy*. John Wiley & Sons, 2006.

[3] D. Pattabiraman, R. H. Lasseter, and T. M. Jahns, "Comparison of grid following and grid forming control for a high inverter penetration power system," in *Proceedings of the IEEE Power & Energy Society General Meeting*, Portland, USA, 5-10 August 2018.

[4] S. Bacha, D. Picault, B. Burger, I. Etxeberria-Otadui, and J. Martins, "Photovoltaics in microgrids: An overview of grid integration and energy management aspects," *IEEE Industrial Electronics Magazine*, pp. 33-46, 2015.

[5] P. Denholm and R. M. Margolis, "Evaluating the limits of solar photovoltaics (PV) in electric power systems utilizing energy storage and other enabling technologies," *Energy Policy*, vol. 35, no. 9, pp. 4424-4433, 2007.

[6] J. G. de Matos, F. S. F. e. Silva, and L. A. de S. Ribeiro, "Power control in AC isolated microgrids with renewable energy sources and energy storage systems," *IEEE Transactions on Industrial Electronics*, vol. 62, no. 6, pp. 3490-3498, 2015.

[7] H. Mahmood, D. Michaelson, and J. Jiang, "A power management strategy for PV/battery hybrid systems in islanded microgrids," *IEEE Journal of Emerging and Selected Topics in Power Electronics*, vol. 2, no. 4, pp. 870-882, 2014.

[8] H. Cai, J. Xiang, M. Z. Q. Chen, and W. Wei, "A decentralized control strategy for photovoltaic sources to unify MPPT and DC-bus voltage regulation," in *The 2017 American Control Conference (ACC)*, 24-26 May 2017.

[9] A. Elrayyah, Y. Sozer, and M. E. Elbuluk, "Modeling and control design of microgrid-connected PV-based sources," *IEEE Journal of Emerging and Selected Topics in Power Electronics*, vol. 2, no. 4, pp. 907-919, 2014.

[10] A. Elrayyah, Y. Sozer, and M. Elbuluk "Microgrid-connected PV-based sources: A novel autonomous control method for maintaining maximum power," *IEEE Industry Applications Magazine*, pp. 19-29, 2015.

[11] H. Liu,, Y. Yang,, X. Wang,, P.C. Loh,, F. Blaabjerg,, W. Wang, and D. Xu,, "An enhanced dual droop control scheme for resilient active power sharing among paralleled two-stage converters," IEEE Transactions on Power Electronics, vol. 32, no. 8, 2017, pp. 6091-6104.

[12] B. B. Johnson, S. V. Dhople, A. O. Hamadeh, and P. T. Krein, "Synchronization of parallel single-phase inverters with virtual oscillator control," *IEEE Transactions on Power Electronics*, vol. 29, no. 11, pp. 6124-6138, 2014.

[13] S. V. Dhople, B. B. Johnson, and A. O. Hamadeh, "Virtual oscillator control for voltage source inverters," in *The 51st Annual Allerton Conference on Communication, Control, and Computing*, 2-4 October 2013.

[14] B. B. Johnson, M. Sinha, N. G. Ainsworth, F. Dörfler, and S. V. Dhople, "Synthesizing virtual oscillators to control islanded inverters," *IEEE Transactions on Power Electronics,* vol. 31, no. 8, 2016, pp. 6002-6015, 2016.

[15] G. S. Seo, M. Colombino, I. Subotic, B. Johnson, D. Gross, and F. Dorfler, "Dispatchable virtual oscillator control for decentralized inverter-dominated power systems: analysis and experiments,"

in *The 2019 IEEE Applied Power Electronics Conferences*, Anaheim, California, 17–21 March 2019.

[16] M. A. Awal, H. Yu, H. Tu, S. Lukic, and I. Husain, "Hierarchical control for virtual oscillator based grid-connected and islanded microgrids," *IEEE Transactions on Power Electronics*, vol. 35, no.1, pp. 988-1001, Jan. 2020.

[17] B. Johnson, M. Rodriguez, M. Sinha, and S. Dhople, "Comparison of virtual oscillator and droop control," in *The 2017 IEEE 18th Workshop on Control and Modeling for Power Electronics*, 9-12 July 2017.

[18] B. B. Johnson, S. V. Dhople, J. L. Cale, A. O. Hamadeh, and P. T. Krein, "Oscillator-based inverter control for islanded three-phase microgrids," *IEEE Journal of Photovoltaics*, vol. 4, no. 1, pp. 387-395, 2014.

[19] A. E. W. H. Kahlane, L. Hassaine, and M. Kherchi, "LCL filter design for photovoltaic grid connected systems," *Journal of Renewable Energies*, pp. 227-232, 2014.

[20] H. Guldemir, "Sliding mode control of DC-DC boost converter," *Journal of Applied Sciences*, vol. 5, no. 3, pp. 588-592, 2005.

[21] J. Zhang, D. G. Dorrell, L. Li, and A. Argha, "A novel sliding mode controller for DC-DC boost converters under input/load variations," in The 41st Annual Conference of the IEEE Industrial Electronics Society, 9-12 November 2015.

[22] C. Asma, Z. Abdelaziz, and Z. Nadia, "Dual loop control of DC-DC boost converter based cascade sliding mode control," in *The 2017 International Conference on Green Energy Conversion Systems*, 23-25 March 2017.

[23] J. Liu, "Basic sliding mode control principle and design," in *Sliding Mode Control Using MATLAB*, J. Liu, Ed. Academic Press, 2017, ch. 1, pp. 1-29.

[24] R. I. Putri, S. Wibowo, and M. Rifa'i, "Maximum power point tracking for photovoltaic using incremental conductance method," *Energy Procedia*, vol. 68, pp. 22-30, 2015.

[25] S. R. Chafle and U. B. Vaidya, "Incremental conductance MPPT technique FOR PV system," *International Journal of Advanced Research in Electrical, Electronics and Instrumentation Engineering*, vol. 2, no. 6, pp. 2720-2726, 2013.

[26] O. Palizban, K. Kauhaniemi and J. M. Guerrero, "Evaluation of the hierarchical control of distributed Energy Storage Systems in islanded Microgrids based on Std IEC/ISO 62264," in *The 2016 IEEE Power and Energy Society General Meeting (PESGM)*, Boston, USA, 17-21 July 2016.

[27] O. Palizban, K. Kauhaniemi, and J. M. Guerrero, "Microgrids in active network management–part II: System operation, power quality and protection," *Renewable and Sustainable Energy Reviews*, vol. 36, pp. 440-45, 2014.

[28] *IEEE Standard for Interconnection and Interoperability of Distributed Energy Resources with Associated Electric Power Systems Interfaces*, IEEE Std 1547-2018, New York, 2018.

Han Min Htut received his B.Eng degree in Electrical Power Engineering from Pyay Technological University, Myanmar in 2014. Currently, he is studying M.Eng Program in Electrical Power and Energy Engineering at the Sirindhorn International Thai-German Graduate School of Engineering, King Mongkut's University of Technology North Bangkok and he has completed his internship and master thesis research at the Institute for Automation of Complex Power System within the E.ON Energy Research Center at RWTH Aachen University, Germany. His research interests include integration of distributed generation systems (DGs), and power system stability.

Wijarn Wangdee received the B.Eng. degree from Chulalongkorn University, Thailand, in 1999 and the M.Sc. and Ph.D. degrees from the University of Saskatchewan, Canada, in 2002 and 2005, respectively. From 2006 to 2013, he worked as a system planning engineer at BC Hydro and Power Authority in Vancouver, Canada. He is currently an associate professor at the Sirindhorn International Thai-German Graduate School of Engineering (TGGS), King Mongkut's University of Technology North Bangkok (KMUTNB), Bangkok, Thailand. He is a senior member of the IEEE. His research interests include power grid reliability, renewable energy and storage system integration, power grid analytics and automation.